

ADAPTIVE IMAGE SUPER-RESOLUTION ALGORITHM BASED ON FRACTIONAL FOURIER TRANSFORM

AHMAD FARAMARZI^{✉,1}, ALIREZA AHMADYFARD² AND HOSSEIN KHOSRAVI³

¹Department of Electrical Engineering, Shahrood University of Technology, Iran; ²Department of Electrical Engineering, Shahrood University of Technology, Iran; ³Department of Electrical Engineering, Shahrood University of Technology, Iran

e-mail: AhmadFaramarzi@shahroodut.ac.ir; ahmadyfard@shahroodut.ac.ir;

HosseinKhosravi@shahroodut.ac.ir

(Received April 27, 2022; revised June 25, 2022; accepted June 27, 2022)

ABSTRACT

Super-resolution imaging is a critical image processing stage that improves visual image quality. Super-resolution imaging has a wide array of use in different fields, such as medical, satellite, and astronomical images. The correct execution of this stage could increase the accuracy and quality of any available processes in different executive fields. Learning methods, especially deep learning, have become much more popular in recent years for performing the super-resolution imaging process. Methods with this approach have high-quality levels but lack appropriate performance times. This study intends to perform super-resolution imaging using an algorithmic approach based on the particle swarm optimization algorithm and the fractional Fourier transform. The test results on a dataset show the 92.16 % accuracy of this proposed method.

Keywords: fractional Fourier transform, image enhancement, particle swarm optimization algorithm, super-resolution imaging.

INTRODUCTION

The technological progress of imaging in different devices, such as home screens, mobile phones, satellite imaging systems, medical imaging systems, and all monitoring systems (including road cameras and astronomy imaging systems), created the need for high-resolution images. There are two major approaches to providing this necessary requisite in practical situations: the first is using proper hardware based on the intended usage, and the second is using software processes to increase the image resolution. The development of artificial intelligence and its different branches (such as machine learning, digital image processing, and machine vision) lead to the popularity of the second approach (using software algorithms) for creating high-resolution images. There have been many studies regarding the usage of machine learning, especially deep learning, in super-resolution imaging in recent years (Liu *et al.*, 2018; Yang *et al.*, 2019; Li *et al.*, 2021; Liu *et al.*, 2020).

However, deep learning methods suffer from complex computations and data dependency in their final model. In other words, super-resolution imaging models are limited to that problem's data in model training. Furthermore, deep learning methods mostly

have a hidden parametric structure instead of an algorithmic nature, which means users are unaware of their background operations. Therefore, presenting an algorithmic method for image quality enhancement using super-resolution imaging becomes important. The current study intends to address this problem.

Many techniques with simple approaches avoid deep learning for super-resolution image recreation (Park *et al.*, 2003; Park, 2004). The super-resolution imaging studies presented in this article use deep learning approaches because this study intends to compare its proposed method's operational generality with deep learning-based methods. Super-resolution imaging based on deep learning consists of supervised and unsupervised network learning mechanism (Wang *et al.*, 2020). Both mechanism use deep convolutional networks as their base (Fang *et al.*, 2020; Suseela and Kalimuthu, 2021; Liu *et al.*, 2019; Troung *et al.*, 2019; Weiss *et al.*, 2019). Convolutional networks are a significant component of deep networks such as Unet (Fang *et al.*, 2020) or are used as a generative adversarial network (Liu *et al.*, 2019).

(Fang *et al.*, 2020), is the first considered study that uses deep learning with a supervised model for super-resolution imaging. They perform super-

resolution imaging on cellular images. They use low-resolution images from a spot scanning system, a deep network, and a designed reducer to reduce the resolution of high signal to noise ratio (SNR) groundtruth images while teaching a system to increase the quality of respective groundtruth images with low resolution. This study uses a deep Unet network with a resNet-34 basis. This method can achieve higher learning speeds for produced data because of its resolution reducer.

(Hatvani *et al.*, 2018), used a deep convolutional base inside a deep Unet network to improve dental texture damage images. They used a dental tomography image dataset alongside a deep convolutional network to improve microscopic CT-Scan images for improved dental root canal injury diagnosis. The usage of various super-resolution imaging performance measures is a notable factor in this study. The proposed method results show better root canal, size, and shape diagnoses while using deep convolutional networks.

(Truong *et al.*, 2019) is another study that uses a deep learning system to improve the resolution of images from a visible light camera used in a drone for landing. Implementing the deep convolutional network on two different datasets shows the proposed method's proper performance in using the executive system in drones.

Another study from (Liu *et al.*, 2019) uses a generative adversarial network to improve images with limited pixel counts and diffraction limitations. The results show the system's cohesive super-resolution imaging capabilities in chips and its usage for improving microscopic holographic images.

These studies generally show the target-oriented super-resolution imaging process in different applications to improve the target system's performance. Implementing deep learning and deep convolutional networks is an effective approach to image quality enhancement and their super-resolution imaging process. However, deep learning has the following challenges even with its high accuracy levels:

1. System learning requires sample datasets
2. The main operations are performed in a black box hidden from the writer.
3. The high computational complexity and slow algorithmic speed.

Regarding the discussed challenges of super-resolution imaging activities based on deep learning in different areas, our proposed method will somewhat

address the three challenges of the numerous dataset requirement, high time complexity, and algorithmic resolution in how to perform super-resolution imaging. For the first challenge regarding the large number of datasets, our proposed method is a simple routine, including a set of basic image processing commands that directly perform super-resolution imaging on the input image. Therefore, learning is not required in the process. On the other hand, it can be asserted that the computational complexity of the proposed method is significantly lower than deep learning-based approaches due to the simplicity and low computational complexity of each executive step of the super-resolution imaging routine. Regarding the fact that the proposed method is a sequential routine of simple image processing commands, it can be said that the proposed method can be outlined as a step-by-step algorithm, and the output of each step can be observed. Therefore, how the method functions is adequately transparent. In addition to all the discussed issues of the deep learning-based methods, the most important disadvantage of algorithmic super-resolution imaging approaches is the low accuracy and quality of the target process. Our proposed method improves the accuracy and quality of algorithmic methods due to its internal structure.

The rest of this study is structured as follows. The second section presents the generalities of the proposed super-resolution imaging algorithmic method. The third section discusses the proposed method's results. In the end, the fourth section presents the discussion.

PROPOSED METHOD

This section will discuss the proposed method in detail. The proposed method consists of three major sections (Fig. 1 depicts this diagram with highlighted major sections). This study will go over two base theoretical concepts used in this algorithm before getting to the proposed method algorithm itself.

FRACTIONAL FOURIER TRANSFORM

The Fourier Transform is a strong mathematical technique that transforms spatial domains into frequency domain signals. The Fourier transform can divide signals into their sine and cosine components regardless of the sound wave and/or image matrix. Equations 1 and 2 present the mathematical Fourier transform equation. Equation 1 determines the discrete Fourier transform, and Equation 2 the continuous Fourier transform for a determined signal.

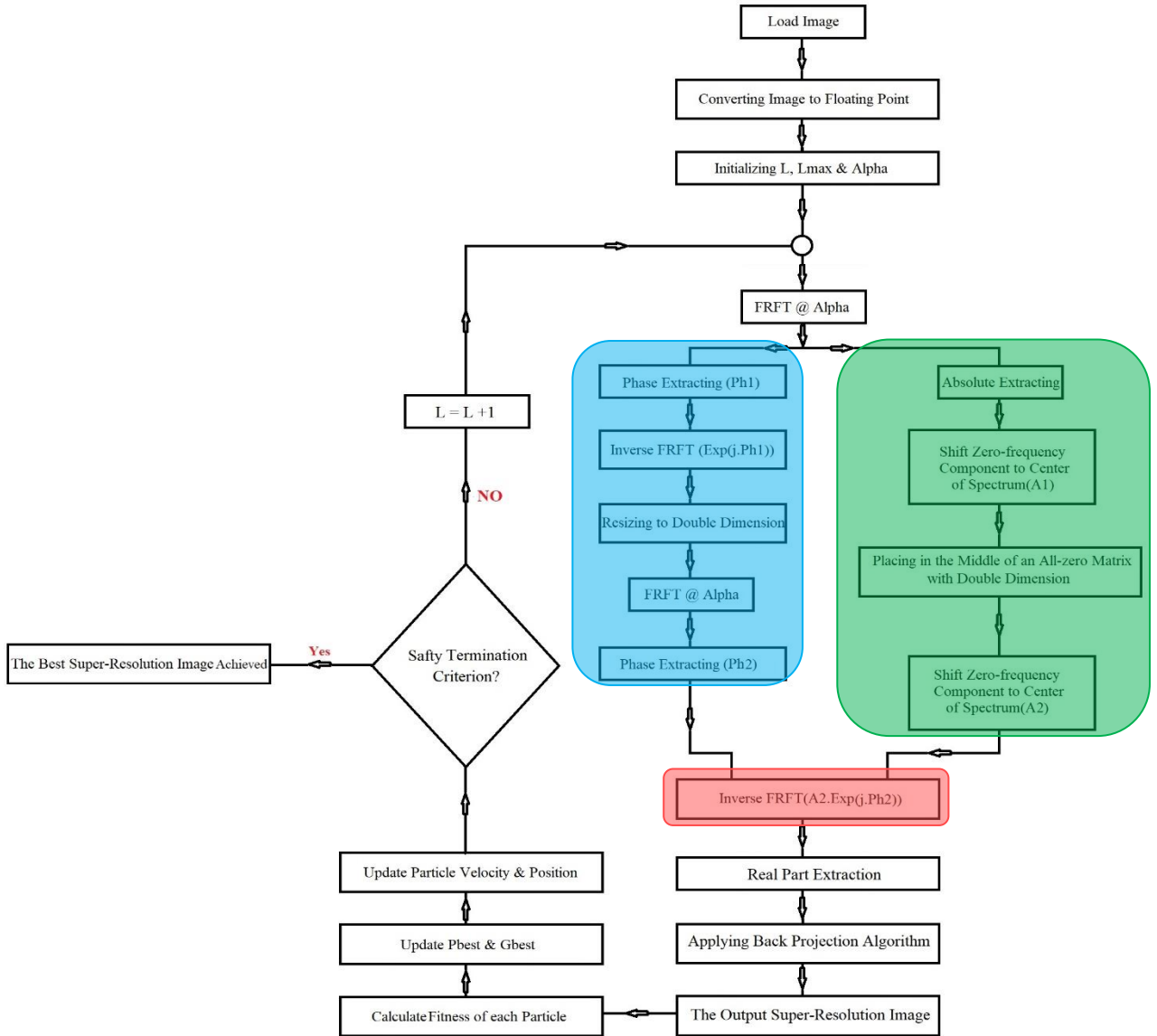


Fig.1. Adaptive Fractional Fourier Super-Resolution(AFFSR) Method's Diagram

$$X(\omega) = \sum_{n=-\infty}^{n=+\infty} x(n)e^{-j\omega n} \tag{1}$$

$$X(\omega) = \int_{-\infty}^{+\infty} x(t)e^{-j\omega t} dt \tag{2}$$

The fractional Fourier transform is a generalized form of the Fourier transform. It is a linear operator defined in (Sejdić *et al.*, 2011; Mendlovic and Ozaktas ,1993; Almeida,1994).

Equation 3 depicts its mathematical nature.

$$X_{\alpha}(u) = F_{\alpha}(x(t)) = \int_{-\infty}^{+\infty} x(t)K_{\alpha}(t.u)dt \tag{3}$$

There $K_{\alpha}(t.u)$ parameter here is defined as follows:

$$K_{\alpha}(t.u) = \begin{cases} \sqrt{\frac{1-j\cot\alpha}{2\pi}} e^{j(\frac{u^2}{2})} \cot\alpha \times e^{j(\frac{t^2}{2})} \cot\alpha - jut \csc\alpha & \text{I} \\ \delta(t-u) & \text{II} \\ \delta(t+u) & \text{III} \end{cases} \tag{4}$$

Section (I) of the $K_{\alpha}(t.u)$ function from Equation 4 is used in Equation 3 when α is not a multiple of π , Section (II) is used when α is a multiple of 2π , and Section (III) is used when $\alpha + \pi$ is a multiple of 2π . Also, δ in this equation is the Dirac delta function (Sejdić *et al.*, 2011). The fractional Fourier transform is the n-th exponentiation of the Fourier transform that

could be mapped onto any time to frequency domain, unlike the normal Fourier transform. In other words, fractional Fourier transforms facilitate the usage of all available gradients in a determined signal. Therefore, the normal Fourier transform will be a special state of its fractional type. Fig. 2 shows the fractional Fourier transform. This approach is widely used in optical problems (Hricha *et al.*, 2020; Saad *et al.*, 2018; Zhao *et al.*, 2018; Dai *et al.*, 2021), image processing (Faragallah *et al.*, 2021; Kaur *et al.*, 2021; Massihi and Rashidi, 2021; Zhang *et al.*, 2021), robotics (Lopez *et al.*, 2021), and medical signal processing (Gupta *et al.*, 2021; Alqahtani *et al.*, 2022; Mastromichalakis and Chountasis, 2021).

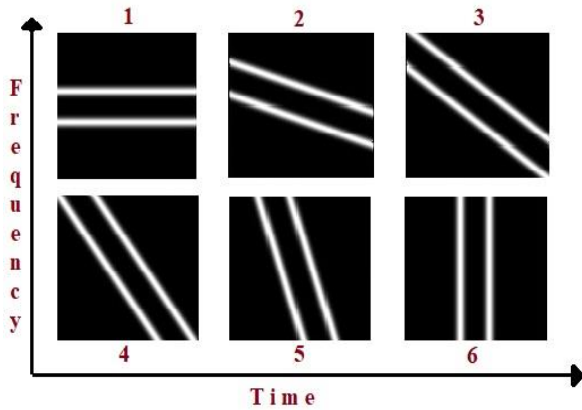


Fig.2. Fractional Fourier Transform's General Nature

PARTICLE SWARM OPTIMIZATION

The particle swarm optimization algorithm is a metaheuristic method presented in 1995 by (Poli *et al.*, 2007). This algorithm can solve complex engineering problems by taking inspiration from the swarm behavior of some phenomena, such as flying birds, (de Moura Meneses *et al.*, 2009). Needing fewer parameters for optimization and high accuracy comprehensive function mapping are two significant benefits of this approach compared to other metaheuristic methods. Fig. 3 shows the general diagram of the particle swarm optimization method.

Particle swarm optimization is a powerful technique for solving many engineering problems. It is a flexible algorithm that can be mixed with other mathematical structures. This study uses particle swarm optimization to find the optimal fractional Fourier transform answer in image enhancement. The following section explains the proposed algorithm for super-resolution imaging considering these two theoretical concepts.

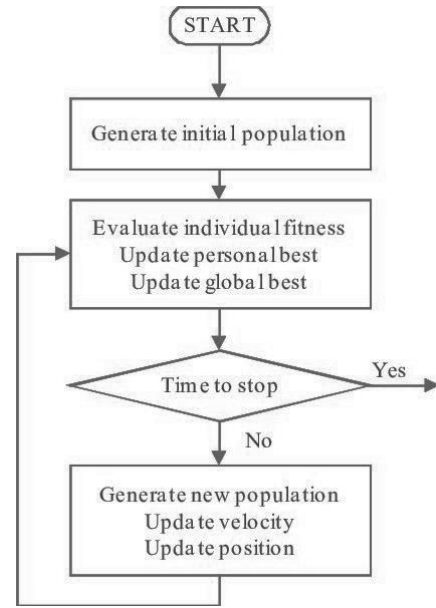


Fig. 3. Particle Swarm Optimization Diagram (Kachitvichyanukul, 2012)

PROPOSED ALGORITHM DETAILS

There are three main blocks in the proposed algorithm (green, blue, and red in Fig. 1). The green and blue blocks parallelly perform a sequential operation set on their input and forward it to the red block. In other words, these three blocks perform the main super-resolution imaging operation as the middle stage of the executive process. The first stage is before these blocks, and the final stage is after the red block's output. The following section discusses this executive algorithm's stage-by-stage process for each diagram stage.

THE INITIAL STAGE

There are three primary operations in this phase after uploading the input image:

1. Transform the image into a floating- point state for future processings.
2. Configure the initial algorithm parameters alongside the corresponding initial particle swarm optimizer parameters
 - a. The general number of algorithm iterations for the super-resolution imaging process.
 - b. Determine the initial particle swarm optimizer algorithm parameters corresponding to the initial population (initial alpha value) and the initial population value.
3. Fractional Fourier transform operation

After executing operations 1 to 3, the output from 3 is forwarded to the green and blue blocks.

THE MIDDLE STAGE

This stage consists of three blocks. The green and blue blocks operate parallelly without any other parametric dependencies. However, the red block is dependent on both. The operational procedure of each block is as follows:

1. The Green Block

- a. Extract the initial phase's output spectrum size from the fractional Fourier transform operation.
- b. Shift the stage (a) matrix to insert the zero-frequency components in the spectrum center.
- c. Insert the shifted stage (b) matrix in the center of a zero matrix twice as large as the current one.
- d. Shift the stage (c) matrix to insert the zero-frequency components in the spectrum center.

Forward the resulting matrix (A2) to the red block.

2. The Blue Block

- a. Extract the previous stage's phase (the initial stage)

Define the Fourier transform from the extracted phases and implement the inverse fractional Fourier transform.

Double the current stage (b) matrix size using the Bi-Cubic method.

Implementing the fractional Fourier transform with the alpha value on the resulted stage (c) matrix.

Extract the stage (d) output spectrum phase and forward it to the red block.

3. The Red Block

- a. Combine the green block (the A2 size matrix) and the blue block (the Ph2 phase matrix) output matrices.

Implement the inverse fractional Fourier transform on the resulted stage (a) matrix to change its domain from frequency to time (space).

THE FINAL STAGE

The red block output is a signal consisting of real and imaginary sections. Only the real section matters for processing. Therefore, the final phase consists of the following steps:

Extract the real section from the middle phase (red block) output signal.

Implement the BackProjection operation on the step 1 output with 100 iterations (the output from step

1 is a matrix two times larger than the input image with low resolution). The output of this step is the first high-resolution image.

Calculate the fitness function.

Update the Pbest and Gbest values.

Update the Alpha that includes particle speed and location values.

Check the algorithm stop condition

If the stop condition is met:

The algorithm ends.

The best super-resolution image and optimized fractional Fourier transform alpha are shown as the final output.

If the stop condition is not met:

The algorithm returns to step 3 of the initial phase and repeats itself with these new values.

There are three crucial notes regarding three super-resolution imaging algorithm stages using the fractional Fourier transform and the particle swarm optimizer algorithm. First, the resolution is used in an algorithmic structure, which is non-existent in deep learning-based algorithms because everything happens in the background of a matrix computation set without the structural resolution of the used algorithm.

Second, the proposed algorithm is computationally more straightforward than other deep learning methods. This significantly increases the proposed method's speed.

ALPHA PARAMETER CALCULATION

The algorithm uses two variables (number of iterations and fitness function derivative value for the particle swarm optimizer) to determine its ending whenever one of them reaches its intended value. The alpha parameter value depends on the particle swarm optimizer fitness function. This study uses the proposed method's percentage of signal to noise ratio(PSNR) output compared to the Bi-Cubic output on the input image (a fixed value) to define the particle swarm optimizer's fitness function. Equation 5 depicts the mathematical nature of PSNR.

$$PSNR(x, y) = 10 \log_{10} \left(\frac{MAX^2}{MSE(x, y)} \right) \quad (5)$$

The mean square error (MSE) parameter used here is calculated using Equation 6.

$$MSE(x, y) = \frac{1}{M * N} \sum_{i=1}^M \sum_{j=1}^N (x - y)^2 \quad (6)$$

The x and y values here are the Bi-Cubic output and super-resolution images. Furthermore, MAX is the highest brightness value in the super-resolution image. Therefore, the PSNR value increases for a fixed value with more super-resolution imaging process iterations. Furthermore, the fitness function must be maximized during the optimization process. Thus, the negative PSNR value must be minimized considering the minimization goal in the particle swarm optimization method, which will maximize the target value. The

proposed particle swarm optimization algorithm stops after receiving a fitness function derivative value lower than 0.001 after multiple consecutive iterations. Fig. 4 depicts the fitness function results after 100 iterations. The application reaches its stop condition after 72 iterations in this figure, with a fitness function value of 41.6847. Furthermore, the optimized alpha value for the fitness function is 0.36432. The following section will present the experimental results of using the proposed method.

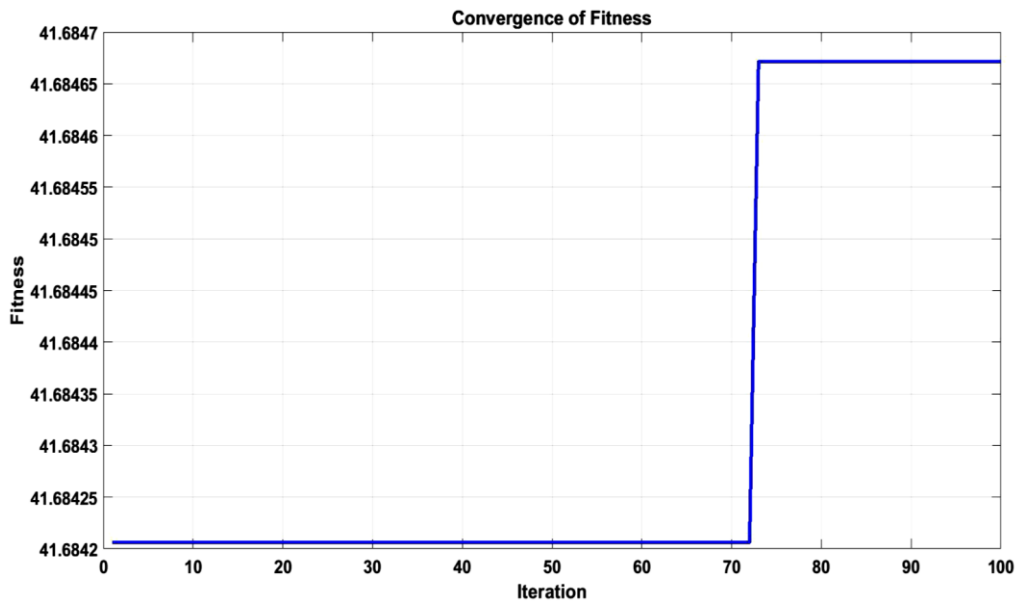


Fig. 4. Particle Swarm Optimizer's Fitness Function Value in the Proposed Method

RESULTS

This section starts by reviewing the proposed method's identification accuracy. Then, it presents a performance comparison between the proposed and other available methods.

IDENTIFICATION ACCURACY

The proposed method's identification accuracy. Furthermore, the average error rates of values from 40 classes were analyzed to better understand the proposed method's classification error rates. The results show an overall average error rate of 7.84 %; therefore, the proposed method has a 92.16 % accuracy. Fig. 5 depicts the error rates for all 40 classes.

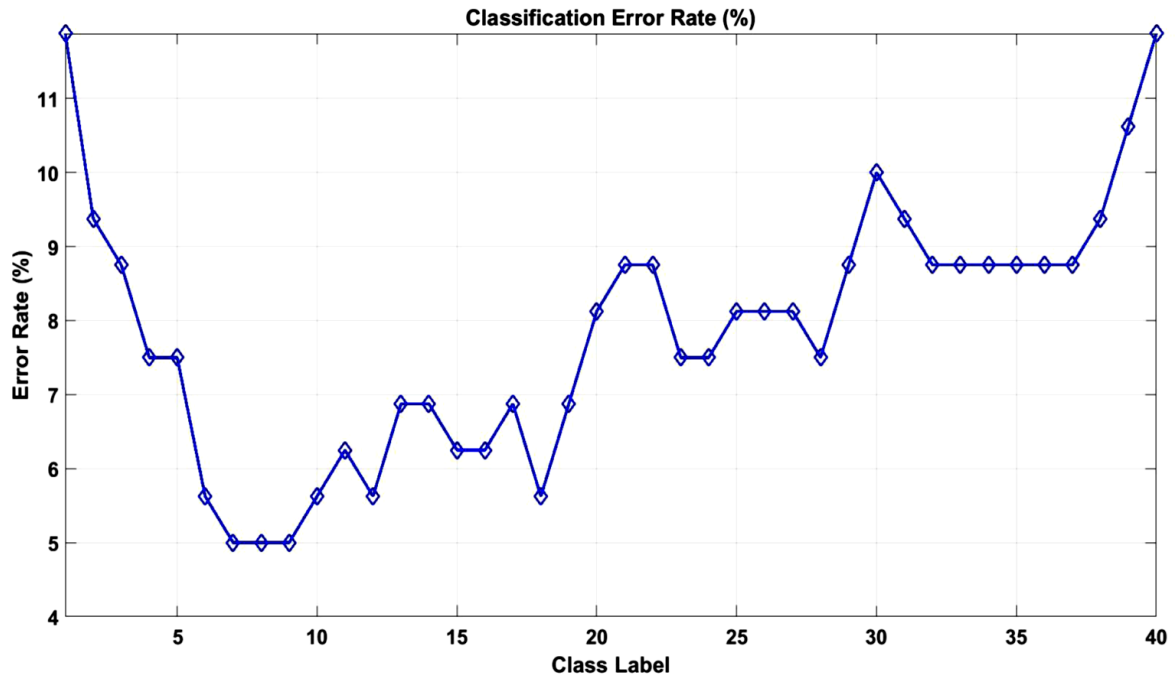


Fig. 5. Average Classification Error Rate for the ORL database

This section analyzes some super-resolution images. Fig. 6 depicts the output of multiple super-resolution images using the proposed method alongside results from the Bi-Cubic method used in the particle swarm optimizer's fitness function. These images show the proposed method's clear advantage over the Bi-Cubic method in depicting image detail. In Fig. 6, first row is original images that resized to 256*256 before super-resolution. The second and Third rows depicts result of Bi-cubic and AFFSR methods respectively. As can be seen, in the super-resolution process using the proposed method, the opacity phenomenon is significantly reduced compared to the Bi-cubic method.

PARAMETERIC COMPARISON

Parametric evaluation criteria are calculable using mathematical equations based on the input and output data. This section compares the proposed methods using the PSNR, Structural Similarity Index Measure (SSIM), and RunTime criteria. The RunTime criterion

indicates the execution time of the super-resolution process for an input image. The lower the value of this criterion, the higher the speed and the lower the computational complexity of the implementation method. Another criterion is SSIM, which is used to measure the structural similarity index. In fact, this criterion determines the quality of the super-resolution image compared to the original image.

Equation 7 indicates the mathematical form of this criterion.

$$SSIM(x, y) = \frac{(2\mu_x\mu_y + c_1)(2\sigma_{xy} + c_2)}{(\mu_x^2\mu_y^2 + c_1)(\sigma_x^2\sigma_y^2 + c_2)} \quad (7)$$

In the above relation, μ_x and μ_y are the pixel means and σ_x^2 and σ_y^2 are pixel variances of the original and super-resolution images. c_1 and c_2 are constant values. The quality of super-resolution process is better when the SSIM is higher.



Fig. 6. A.original images B.Output of Bi-Cubic method C.output of AFFSR method

COMPARISION BY BI-CUBIC ALGORITHM

This section compares the proposed method's PSNR, SSIM, and RunTime values with the Bi-Cubic method in several images. These images enter the super-resolution imaging process with a 256*256 resolution and exit as 512*512. Table 1 depicts the results of this comparison, which shows the definitive superior performance of the proposed AFFSR compared to the Bi-Cubic method in all three criteria.

In the explanation of Table 1, to make a comprehensive and rapid conclusion about the comparison of the proposed method with the Bi-Cubic method in the parameters of RunTime, PSNR, SSIM, the last row of the table with the title of average can be used. As can be seen in this row, the average RunTime for the proposed method is higher than the Bi-Cubic method, while in the average of the other two parameters, a higher value can be seen for the proposed method

compared to the Bi-Cubic method. This higher value indicates that the proposed method produces a higher quality image than the Bi-Cubic method.

COMPARISION BY OTHER METHODS

This section compares the proposed method's performance with other studies using several images. This comparison is between their PSNR values. These images enter the process with a 256*256 resolution and exit as 512*512. Table 2 shows the comparison result. As reported in Table 2, it can be seen that the proposed method has a higher PSNR in most images than the previous methods, but in some images the PSNR value of the AFFSR method is lower than some methods. The conclusion obtained from the average row indicates that the proposed method is in the second place after the Chen method in terms of the quality of the produced image.

Table 1: Comparing the Proposed (AFFSR) and Bi-Cubic Methods

Image	RunTime(sec)		PSNR		SSIM	
	Bi-cubic	Proposed (AFFSR)	Bi-cubic	Proposed (AFFSR)	Bi-cubic	Proposed (AFFSR)
Barbara	0.1519	1.4812	25.3511	25.567	0.6656	0.7278
Barbara2	0.1563	1.4864	27.7831	28.7662	0.7703	0.8228
Boat	0.1420	1.4855	29.9472	30.9054	0.6639	0.7150
Cameraman	0.1364	1.4849	35.7448	38.3443	0.8410	0.8874
Clown	0.1357	1.4597	32.6602	34.1681	0.7368	0.7740
Crowd	0.1499	1.5036	32.6606	34.2721	0.8749	0.9027
Goldhill	0.1518	1.5063	31.4538	32.2247	0.7281	0.7778
Lena	0.1352	1.4590	34.1194	35.4265	0.7174	0.7633
Man	0.1473	1.4886	31.053	32.04	0.7632	0.8108
Mandrill	0.1518	1.6052	23.6416	24.3146	0.6393	0.7242
Peppers	0.1521	1.5011	31.855	32.6989	0.6527	0.6968
SanDiego	0.1442	1.5177	30.1996	31.3127	0.6633	0.7447
Average	0.1462	1.4983	30.5394	31.6700	0.7264	0.7789

Table 2: Comparing PSNR Values of the Proposed Method (AFFSR) with Approaches from Other Studies

Method	Barbara	Man	Boat	Mandrill	Lena	Peppers	Clown	Couple	Cameram.	Crowd	Average
(Li and Ordhard, 2001)	26.47	26.11	25.75	22.92	27.33	26.88	25.82	26.21	25.94	25.51	25.89
(Yang <i>et al.</i> , 2010)	29.33	29.34	28.30	23.93	31.43	31.13	29.34	28.4	29.59	28.92	28.97
(Tsa <i>et al.</i> , 2012)	24.93	24.95	24.51	22.51	25.27	24.78	22.65	25.56	24.91	24.53	24.46
(Chen and Fowler, 2012)	30.61	30.67	29.99	24.76	32.72	31.91	29.91	29.83	31.46	30.96	30.28
(Zhu <i>et al.</i> , 2014)	30.41	30.36	29.72	24.42	32.28	31.81	30.12	29.47	30.96	30.64	30.02
(Freedman and Fattal, 2011)	28.69	29.23	28.79	25	29.91	29.6	28.69	28.62	29.89	28.69	28.71
(Mokari and Ahmadyard, 2017)	30	30.91	29.60	24.61	31.83	32.51	30.14	28.9	30.9	29.98	29.94
Proposed (AFFSR)	30.38	30.82	29.27	26.32	32.37	32.31	29.9	29.22	30.36	29.89	30.09

COMPARING USING FEI FACE DATA

This section compares the proposed method with other studies based on the PSNR, SSIM, and RunTime criteria using six face images (Fig. 7: F1 to F6) from the FEI dataset. Table 3 presents the results. These images enter with a 146*146 resolution and exit the super-resolution imaging process as 292*292. Table 3 clearly depicts the lower RunTime values of the proposed method compared to others. However, the proposed method has a definite advantage over other methods in the PSNR criterion.

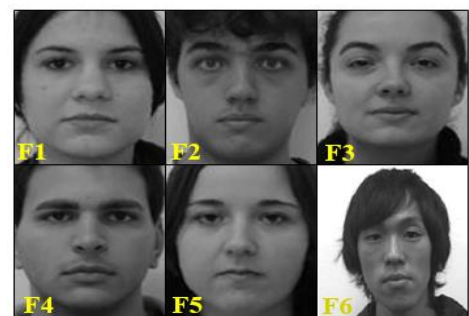


Fig. 7. Face Images from the FEI Databas

Table 3: Comparing the Proposed and Other Methods using Face Images from the FEI Database

Image	Proposed (AFFSR)			LCR (Jiang and Hu ,2014)			SRLSP (Jiang <i>et al.</i> , 2016)			SSR (Jiang <i>et al.</i> , 2016)			TRNR (Jiang <i>et al.</i> , 2016)		
	PSNR	SSIM	Rtime (sec)	PSNR	SSIM	Rtime (sec)	PSNR	SSIM	Rtime (sec)	PSNR	SSIM	Rtime (sec)	PSNR	SSIM	Rtime (sec)
F1	49.6	0.94	0.55	35.15	0.95	4.23	37.61	0.98	19.7	31.57	0.91	152.88	31.82	0.92	1.97
F2	50.32	0.94	0.48	37.1	0.95	4.55	39.81	0.97	23.44	33.58	0.91	145.49	34.12	0.92	1.45
F3	48.65	0.93	0.46	34.38	0.96	4.39	36.59	0.98	25.96	31.38	0.91	161.26	31.06	0.92	1.83
F4	50.31	0.94	0.5	37.41	0.96	4.43	39.59	0.98	22.15	33.15	0.93	163.03	33.85	0.94	1.91
F5	51.46	0.93	0.47	39.03	0.97	4.32	42.32	0.98	20.93	34.45	0.93	149.34	35.12	0.94	1.89
F6	33.39	0.82	0.46	24.58	0.82	4.29	31.5	0.95	20.61	24.47	0.73	148.92	22.09	0.69	1.47
Average	47.29	0.92	0.49	34.61	0.94	4.37	37.90	0.97	22.13	31.43	0.89	153.49	31.34	0.89	1.75

As shown in the results of Table 3, the time complexity as well as the PSNR value of the proposed method performed better than all available methods. The PSNR value obtained by the proposed method is 25% higher than that of the best available method. Using low computational processing techniques such as Fourier transform in the proposed method has led to a very significant reduction in time complexity compared to other methods.

DISCUSSION

The super-resolution imaging process is one of the most practical image processing subjects (it is used in different fields such as traffic systems, astronomy, and medical systems). Super-resolution imaging in these systems must have high accuracy rates with real-time results. Various studies reached these high accuracy rates by focusing on deep learning. However, these methods are relatively slow, making them unusable in real-time systems. On the other hand, algorithmic super-resolution imaging processes face two significant challenges: weak performance and unique initial configurations for diverse executions with different structural features.

This study proposes a novel super-resolution imaging method using an adaptive approach based on a mixture of the fractional Fourier transform and particle swarm optimizer. This method has a dramatic effect on these two significant challenges. This method's visual and quantitative results determine its higher quality, accuracy, and speed in performing super-resolution imaging based on different criteria. The proposed method improved the time complexity and performance

accuracy (as shown by the PSNR measure) compared to other methods. The PSNR provided by our method is compared to the Bi-cubic method in Table 1 and other methods in Table 2. The accuracy and time complexity of the proposed method in super-resolution imaging of face images were compared with other methods in Table 3, in which the significant improvement of both criteria is obvious. Comparing our proposed method's results with other images and methods in Table 3, PSNR was improved by at least 25%, and runtime was reduced by at least 100%. Furthermore, simplicity, operational clarity, and lower computational complexity in producing high-resolution images are other benefits of this method.

REFERENCES

- Almeida LB (1994). The fractional Fourier transform and time-frequency representations. *IEEE Trans. Signal Process.* 42: 3084-91.
- Alqahtani F, Amoon M, El-Shafai W (2022). A Fractional Fourier Based Medical Image Authentication Approach. *Comput. Mater. Contin.* 70:3133-0.
- Chen C, Fowler JE (2012). Single-image super-resolution using multihypothesis prediction. *ASILOMAR*:608-12.
- Dai ZP ,Wang YB, Zeng Q, Pang ZG, Yang ZJ (2021). Propagation and transformation of four- petal Gaussian vortex beams in fractional Fourier transform optical system. *Optik* 245:167644.
- de Moura Meneses AA, Machado MD, Schirru R (2009). Particle swarm optimization applied to the nuclear reload problem of a pressurized water reactor. *Prog. Nucl. Energy* 51:319-26.

- Fang L, Monroe F, Novak SW, Kirk L, Schiavon CR, Yu SB, Zhang T, et al (2021). Deep learning-based point-scanning super-resolution imaging. *Nat. Methods* 18: 406-16.
- Faragallah OS, El-sayed HS, Afifi A, El-Shafai W (2021). Efficient and secure opto-cryptosystem for color images using 2D logistic-based fractional Fourier transform. *Opt Lasers Eng* 137:106333.
- Freedman G, Fattal R (2011). Image and video upscaling from local self-examples. *ACM Trans. Graph.* 30:1-11.
- Gupta V, Mittal M, Mittal V, Chaturvedi Y (2021). Detection of R-peaks using fractional Fourier transform and principal component analysis. *J Ambient Intell Humaniz Comput* :1-12.
- Hatvani J, Horváth A, Michetti J, Basarab A, Kouamé D, Gyöngy M (2018). Deep learning-based super-resolution applied to dental computed tomography. *IEEE trans. radiat. plasma med. sci.* 3:120-8.
- Hricha Z, Yaalou M, Belafhal A (2020). Introduction of a new vortex cosine-hyperbolic-Gaussian beam and the study of its propagation properties in Fractional Fourier Transform optical system. *Opt Quantum Electron* 52:1-18.
- Jiang J, Chen C, Huang K, Cai Z, Hu R (2016). Noise robust position-patch based face super-resolution via Tikhonov regularized neighbor representation. *Inf. Sci.* 367:354-72.
- Jiang J, Chen C, Ma J, Wang Z, Wang Z, Hu R (2016). SRLSP: A face image super-resolution algorithm using smooth regression with local structure prior. *IEEE Trans Multimedia* 19: 27-40.
- Jiang J, Hu R, Wang Z, Han Z (2014). Noise robust face hallucination via locality-constrained representation. *IEEE Trans Multimedia* 16: 1268- 81.
- Jiang J, Ma J, Chen C, Jiang X, Wang Z (2016). Noise robust face image super-resolution through smooth sparse representation. *IEEE Trans Cybern* 47:3991-4002.
- Kachitvichyanukul V (2012). Comparison of three evolutionary algorithms: GA, PSO, and DE. *Ind. Eng. Manag. Syst.* 11: 215-23.
- Kaur K, Jindal N, Singh K (2021). Fractional Fourier Transform based Riesz fractional derivative approach for edge detection and its application in image enhancement. *Signal Process.* 180:107852.
- Li X, Orchard MT (2001). New edge-directed interpolation. *IEEE Trans Image Process* 10:1521- 27.
- Li Y, Sixou B, Peyrin F (2021). A review of the deep learning methods for medical images super resolution problems. *Irbm* 42:120-3
- Liu D, Zhaowen W, Yuchen F, Xianming L, Zhangyang W, Shiyo C, Xinchao W, Thomas SH (2018). Learning temporal dynamics for video super-resolution: A deep learning approach. *IEEE Trans Image Process* 27:3432-45
- Liu H, Ruan Z, Zhao P, Dong C, Shang F, Liu Y, Yang L (2020). Video super resolution based on deep learning: A comprehensive survey. *arXiv.org*: 2007.12928.
- Liu T, De Haan K, Rivenson Y, Wei Z, Zeng X, Zhang Y, Ozcan A (2019). Deep learning-based super-resolution in coherent Imaging systems. *Sci. Rep.* 9: 1-13.
- Lopes AM, Tenreiro Machado JA (2021). Fractional-order sensing and control: Embedding the nonlinear dynamics of robot manipulators into the multidimensional scaling method. *Sensors* 21:7736.
- Massihi N, Rashidi S (2021). Extracting features from wrist vein images using fractional fourier transform for person verification. *Biomed. Phys. Eng. Express* 7:035016.
- Mastromichalakis S, Chountasis S (2021). A Moment Based Fractional Fourier Transform Scheme for MR Image Classification. *Autom. Control. Comput. Sci.* 55:377-87.
- Mendlovic D, Ozaktas HM (1993). Fractional Fourier transforms and their optical implementation. *J Opt Soc Am A Opt Image Sci Vis* 10: 1875-81.
- Mokari A, Ahmadyfard A (2017). Fast single image SR via dictionary learning. *IET Image Process* 11: 135-44.
- Park SC (2004). Super-resolution image reconstruction: a technical overview. *IEEE Signal Process Mag* 13: 1327-44.
- Park SC, Park MK, Kang MG (2003). Super-resolution image reconstruction: a technical overview. *IEEE Signal Process Mag* 20: 21-36.
- Poli R, Kennedy J, Blackwell T (2007). Particle swarm optimization. *Swarm Intell.* 1:1942- 48.
- Saad F, Ebrahim AAA, Khouilid M, Belafhal A (2018). Fractional Fourier transform of double-half inverse Gaussian hollow beams. *Opt Quantum Electron* 50:1-12.
- Sejdić E, Djurović I, Stanković L (2011). Fractional Fourier transform as a signal processing tool: An overview of recent developments. *Signal Process.* 91: 1351-69.
- Suseela K, Kalimuthu K (2021). An efficient transfer learning-based Super-Resolution model for Medical Ultrasound Image. *J Phys Conf Ser* 1964:062050.
- Truong NQ, Nguyen PH, Nam SH, Park KR (2019). Deep learning-based super-resolution reconstruction and marker detection for drone landing. *IEEE Access* 7:61639-55.

- Tsai CY, Huang DA, Yang MC, Kang LW, Wang YCF (2012). Context-aware single image super-resolution using locality-constrained group sparse representation. *VCIP* :1-6
- Wang Z, Chen J, Hoi SC (2020). Deep learning for image super-resolution: A survey. *IEEE Trans. Pattern Anal. Mach. Intell.* 43: 3365-87
- Weiss S, Chu M, Thuerey N, Westermann R (2019). Volumetric isosurface rendering with deep learning-based super-resolution. *IEEE Trans Vis Comput Graph* 27,3064-78
- Yang MC, Chu CT, Wang YCF(2010). Learning sparse image representation with support vector regression for single-image super-resolution. *IEEE Int. Conf. Signal Image Processing Appl.*: 1973-76
- Yang W, Zhang X, Tian Y, Wang W, Xue JH, Liao Q (2019). Deep learning for single image super-resolution: A brief review. *IEEE T MULTIMEDIA* 21:3106-21.
- Zhang Y, Zhang L, Zhong Z, Yu L, Shan M, Zhao Y (2021). Hyperchaotic image encryption using phase-truncated fractional Fourier transform and DNA-level operation. *Opt Lasers Eng* 143:106626.
- Zhao MD, Gao XZ, Pan Y , Zhang G L, Tu C , Li Y, Wang HT (2018). Image encryption based on fractal-structured phase mask in fractional Fourier transform domain. *J Opt* 20:045703.
- Zhu Z, Guo F, Yu H, Chen C (2014). Fast single image super-resolution via self-example learning and sparse representation. *IEEE Trans Multimedia* 16: 2178-90.